Magnetoresistance and magnetic properties of Fe/Cu/Fe/GaAs(100)

T. L. Monchesky, B. Heinrich, R. Urban, and K. Myrtle
Department of Physics, Simon Fraser University, Burnaby, British Columbia, Canada V5A 1S6

M. Klaua and J. Kirschner
Max-Planck-Institut für Mikrostrukturphysik, Weinberg 2, D-06120 Halle/Saale, Germany
(Received 17 February 1999)

A procedure for growth of smooth As free Fe surfaces on (4×6)-GaAs(100) is presented. Ferromagnetic resonance (FMR) revealed that the Fe films have anisotropies equal to bulk Fe, modified only by interface anisotropies. The Fe films served as templates for the growth of epitaxial Fe/Cu/Fe trilayers which were subsequently characterized by FMR, magneto-optical Kerr effect, and magnetoresistance. At room temperature, films coupled through a 13.2-ML Cu spacer exhibited 2.0% giant magnetoresistance and 0.3% anisotropic magnetoresistance. The results showed that the interlayer exchange coupling for a 13.2-ML Cu spacer could not be described by bilinear and biquadratic contributions alone. A different coupling, which varied as cosine cubed of the angle between the magnetizations of the Fe films, was required to explain the data (bicubic exchange coupling). [S0163-1829(99)05037-7]

I. INTRODUCTION

Most giant magnetoresistance (GMR) studies to date have been carried out on samples of lesser quality than is typically possible with metallic systems. Although the first GMR studies were performed on molecular-beam epitaxy (MBE) grown samples, a larger portion of the studies to date have been prepared by sputtering. This has enabled a larger survey of the magnetoresistance of multilayered systems than would otherwise be possible. MBE, however, enables a better control over interfaces, which has been identified as the region responsible for GMR.[1]

The lack of high quality structures for GMR studies is in part due to difficulties associated with metallic growth on insulating substrates. One of the difficulties presented by Fe growth on GaAs(100) is that the Ga and As diffuse into the metal overlayers and As segregates to the surface.[2] This problem has been addressed by growth on sulfurpassivated surfaces[3] and ozone treated surfaces.[4] In the case of sulfur passivation, the sulfur acts as a surfactant, instead of the As, preventing any diffusion of Ga or As into the Fe layer. However, even in the case of metal-organic chemical vapor deposition (MOCVD) passivated surfaces, which have atomic high, micron wide terraces, reflection high-energy electron diffraction (RHEED) indicates that the segregation of S results in a rough Fe growth.[5]

The magnetic properties of Fe overlayers on GaAs are sensitive to both substrate preparation and growth conditions. On unpassivated GaAs(100) surfaces, the amount of As and Ga out diffusion into the Fe has been shown to be dependent on the substrate temperature and to affect the magnetization. Fe grown on GaAs(100) surfaces prepared by thermally desorbing the native oxide shows evidence for an $Fe_3Ga_{2-x}As_x$ pseudocubic hexagonal phase at the metal-semiconductor interface with half the bulk magnetization of bulk iron.[6] Magnetometry measurements indicate that this ternary is 10 monolayers (ML) thick for 50 °C deposition, whereas it increases to 70 ML for deposition temperatures above 200 °C.

Sputtering and annealing GaAs(100) eliminates the damage created by the desorption of native oxides. Low-energy sputtering is, however, required to minimize the damage created by sputtering since the original surface quality cannot be recovered by annealing as is typically the case for metals. Scanning tunneling microscopy (STM) studies show that 500-eV Ar^+ sputtering and annealing results in a respectable surface quality with terraces 50 nm wide. Room-temperature growth of Fe on (4×6) GaAs(100) prepared in this fashion prevents any magnetic dead layer formation;[7] *ex situ* magnetometry measurements show that the onset of ferromagnetism occurs at the first monolayer. A magnetic moment per atom of $2.1\mu_B$ at the Fe/GaAs(100) interface is inferred from a 7-ML film.

By thermally desorbing a thick As cap from a homoepitaxially grown GaAs(100), Xu *et al.* were able to prepare (4×6) GaAs(100) substrates without introducing sputter damage.[8] *In situ* magneto-optical Kerr effect (MOKE) measurements show an evolution of the magnetic phase as a function of thickness. For thin films less than 3.5 ML thick, the Fe is nonmagnetic. The thickness dependence after the onset of ferromagnetism at 4.5 ML suggests that the Fe layer recovers its full magnetic moment with no magnetic dead layers.

For Fe grown on any of the various GaAs surfaces mentioned above, a large in-plane uniaxial anisotropy is present. The direction of the uniaxial anisotropy is dependent on sample preparation conditions.[7,9–12] Speculations have been made as to its origin, however conclusive evidence has not yet been presented. One feature common to all of these studies is that the uniaxial easy axis is perpendicular to the direction of the dangling bonds. Ga-terminated and As-terminated surfaces have easy uniaxial axes along [1-10] and [110] directions, respectively.

In this paper, a procedure will be presented to produce clean, high quality Fe surfaces with large atomic terraces on

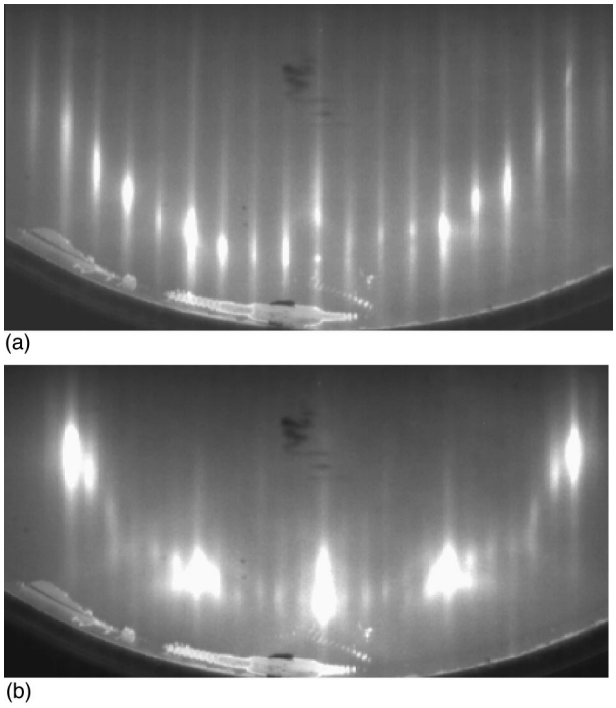

FIG. 1. RHEED pattern (4×6)-GaAs(100) prepared by sputtering and annealing. (a) with the RHEED beam perpendicular to [1-10] and (b) perpendicular to the [110].

Ga-rich (4×6)-GaAs(100). The GaAs(100) is prepared by sputtering in a fashion similar to Gester *et al.*[10] Similar to all Fe growths on GaAs(100), As segregates to the Fe surface and leads to a degradation in the surface quality. This is in contrast to recent reports which show for particular cases surfactants have an advantageous smoothing effect for epitaxial growth, as shown in Ref. 13. By removing the As using low-energy sputtering, it will be shown that higher quality Fe surfaces are obtained. The Fe layers produced by this procedure serve as good templates for growing structures for transport studies. In particular, this paper examines the giant magnetoresistance produced in exchange coupled Fe/Cu/Fe trilayers.

II. GROWTH

A. Substrate preparation

Samples prepared for magnetic characterization were grown on n^+ GaAs(100). For transport measurements, semi-insulating GaAs was used. The GaAs surface was prepared by inserting an epiready American Xtal Technology wafer into UHV without prior treatment and annealed at roughly 500 °C to outgas the sample holder and desorb the carbon. The sample's in-plane angle was rotated while the oxide was removed by 500-eV Ar^+ sputtering at an angle of 75° with respect to the surface normal. The sputtering was performed at room temperature under Auger observation until the contaminants were removed. The sample was then transferred to the growth chamber in order to monitor the surface reconstruction with RHEED while annealing the sample. The sample temperature was raised in 10° steps until a well ordered $p(4\times6)$ reconstruction was obtained as shown in Fig. 1. The temperature was estimated to be roughly 600 °C at this point. The RHEED streaks were short and narrow indicating that the sample's atomic terraces are wide. The superlattice streaks were arranged in a circle. This may be understood in terms of an Ewald sphere intersecting the reciprocal lattice rods. The fact that narrow rods may describe the reciprocal lattice is an indication of a well ordered surface.

B. Fe/GaAs(100)

Fe was deposited on room-temperature GaAs from a resistively heated piece of Fe in a base pressure of 1×10^{-10} Torr. The rate of deposition was roughly 1 Å/min as determined by a quartz-crystal monitor. The RHEED beam was set to the first anti-Bragg condition for Fe, at a polar angle of 1° glancing incidence. The azimuthal angle was set to 0.8° away from the [1-10] direction in order that Kikuchi lines not overlap with the specular spot. Under these conditions, the intensity of the specular spot oscillated during the growth with a one monolayer period, allowing accurate determination of the Fe thickness. For the first two monolayers, the Fe growth proceeds in a Volmer-Weber fashion where wide RHEED streaks due to Fe islands and the 4×6 reconstruction from the GaAs surface are both visible. By the third monolayer evidence of the GaAs surface has disappeared, and by the fifth monolayer the RHEED intensity increased as a result of the coalescence of the Fe islands. Quasi-layer-by-layer growth, for which a second layer nucleates prior to the completion of a first layer, was observed for a thickness greater that 5 ML, as indicated by the RHEED oscillations that persisted beyond 20 ML. Shown in Fig. 2(b) is the splitting of the RHEED streak for a RHEED beam perpendicular to the [110] direction giving a terrace spacing of 40 Å in the [110] direction for a 20.5-ML Fe film. The splitting in Fig. 2(c) could not be resolved along the [1-10] direction, however the streak width is comparable to that in Fig. 2(b). Recent STM studies have shown for a 20-ML Fe film on (4×6)-GaAs(100), the islands are separated by 40 Å in both in [1-10] and [110] directions.[14] The Fe growth presented here is similar to that on (2×4)-GaAs(100),[15] where STM studies show for 35 ML of Fe, the islands are 50×80 Å elongated along the [1-10] direction.

The chemical evolution of the Fe film was monitored using x-ray photoelectron spectroscopy (XPS). Measurements were recorded with a PHI 10-360 analyzer providing a 0.8-eV energy resolution. A shoulder with 1.15 eV±0.20 eV lower binding energy than the Ga $3d$ peak is visible. This shoulder is attributed to Fe-Ga bonding, in agreement with the 1.1-eV shift obtained by Chambers *et al.*[2]

Arsenic segregated to the Fe surface for all Fe growths on GaAs(100) regardless of the substrate reconstruction or preparation. The segregation was most easily observed by the 162-eV kinetic energy As $2p_{3/2}$ XPS line. A comparison of the integrated As and Fe XPS peaks indicated that there was 0.75 ML of As. Further evidence of the segregation was given by the weak $c(2\times2)$ reconstruction as seen by RHEED. In order to remove the As surfactant from 20-ML Fe/GaAs(100), the films were sputtered with 500-eV Ar^+ at an angle of 75° with respect to the surface normal. The sample was rotated around its normal during sputtering. The As $2p_{3/2}$ line was used to monitor the amount of As at the surface; the sputtering was stopped once this peak disap-

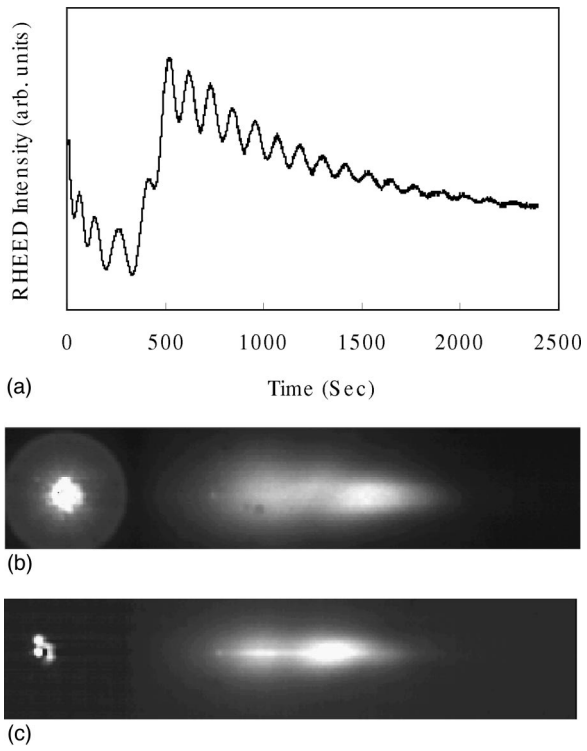

FIG. 2. (a) RHEED intensity oscillations during the growth of Fe/(4×6)-GaAs(100) at room temperature. The polar angle was set to 1° glancing incidence, the first anti-Bragg condition for Fe. (b) The RHEED specular spot for the beam perpendicular to the [110] direction. The splitting of the RHEED streak gives a mean terrace separation of 62 Å. (c) RHEED specular spot for the beam perpendicular to the [1-10] direction.

peared. In the process of cleaning the surface, 2.2 ML of Fe was removed as determined from the decrease in the Fe $2p_{3/2}$ peak. The Ga $2p_{3/2}$ peak [which has an 8-Å inelastic mean free path in Fe (Ref. 16)] increased during the sputtering suggesting that some Ga diffused into the Fe as a result of cascade mixing.[17] Depending on whether the Ga is assumed to be in the first 10 ML, linearly distributed or homogeneously distributed, XPS intensities indicate that there was in total between 0.2 and 0.3 ML of Ga released into the Fe layer as a result of the sputtering.

In order to anneal the damage created by sputtering, the sample was heated while monitoring the Ga and As XPS lines. The temperature could be raised to 200 °C without any out diffusion of As or Ga into the Fe layer, as was the case of Fe grown on S-passivated GaAs(100) substrates.[3] 75-ML-thick $Fe_3Ga_{2-x}As_x$ layers have been observed for depositions at substrate temperatures above 200 °C.[6] In post-deposition annealing of room-temperature growths the bulk diffusion activation energy prevents alloy formation.

The sample was then transferred back to the growth chamber. RHEED showed that the $c(2\times2)$ reconstruction had been removed, however, there was only a small improvement in the quality of the RHEED pattern. By growing at 200 °C, the quality of the surface was significantly improved, as indicated by an increase in the specular spot intensity, an increase in the amplitude of the RHEED oscillations and a narrowing of the RHEED streaks. The end result

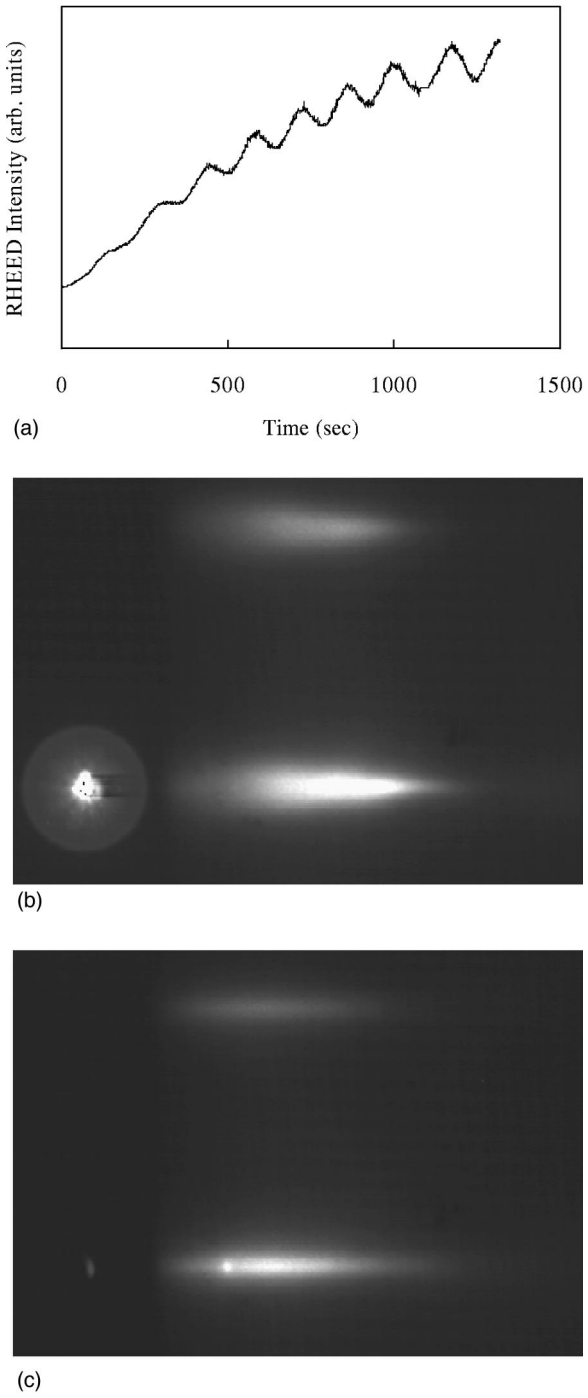

FIG. 3. (a) RHEED intensity oscillations of 9-ML Fe grown on 20-ML-Fe/(4×6)-GaAs(100) at 200 °C. (b) RHEED pattern of 20-ML-Fe/(4×6)-GaAs(100) prior to 200 °C Fe growth. (c) RHEED pattern of 27-ML-Fe/(4×6)-GaAs(100).

was an Fe surface, free of As contamination with large atomic terraces as illustrated by the narrow RHEED streaks in Fig. 3(c).

C. Cu/Fe/GaAs(100)

The high quality Fe(100) templates on GaAs(100) enabled the growth of trilayers for magnetoresistance studies. From Cu growths on Fe templates deposited on Ag(100),[18] it

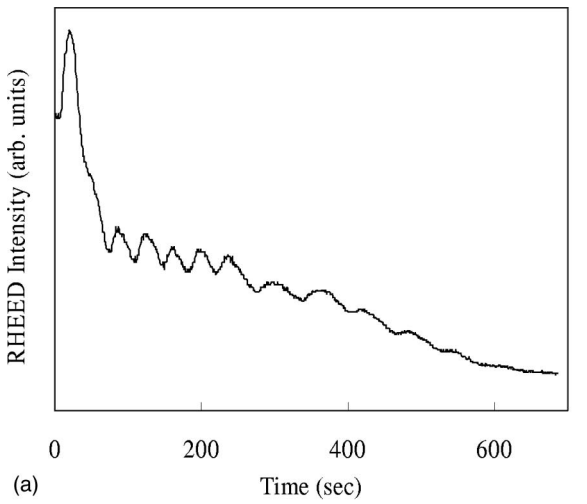

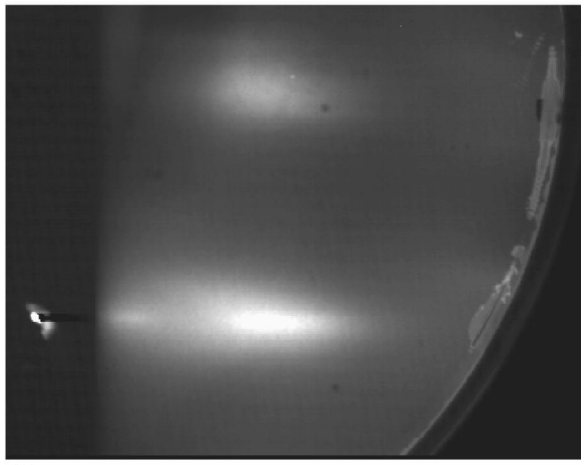

FIG. 4. (a) RHEED intensity oscillations of Cu/28-ML-Fe/(4 $\times$6)-GaAs(100) grown at 85 K. The polar angle was again set to the same anti-Bragg condition as was used for Fe. (b) The RHEED pattern from the Cu surface after 13 ML have been deposited.

is known that Cu grows epitaxially with a bcc structure up to 12 ML. The growth of Cu on Fe/GaAs(100) was expected to have a similar behavior. At room temperature, the RHEED specular spot oscillated for one monolayer, but then rapidly fell in intensity with a corresponding large increase in streak width. At this point the growth was no longer epitaxial: the Cu collected in mounds on the surface leading to wide three-dimensional features in the RHEED pattern. It is interesting to note that this result was also observed in recent STM studies on Fe(100) whiskers[19] in which Cu was found to form nanoscopic crystallites on the Fe surface. This growth mode could be suppressed by cooling the substrate to 85 K and thereby lowering the diffusion length of adsorbed Cu atoms. In this case RHEED oscillations persisted up to 14 ML. There was an initial decrease in specular spot intensity, however, reasonable oscillations continued up to 6 ML after which their amplitude and the intensity of the specular spot decreased (see Fig. 4). As is the case for Cu/Fe/Ag(100) structures with a Cu thickness greater 11 ML, a reconstruction was visible with RHEED. Extended x-ray-absorption fine structure (EXAFS) studies have shown that Cu gradually evolves with increasing thickness into its bulk fcc structure.[20] The Cu/Fe/GaAs samples were capped with a protective 20-ML-thick Cr film in order to perform anisotropy measurements *ex situ*.

D. Fe/Cu/Fe/GaAs(100)

Four Au/Fe/Cu/Fe/GaAs trilayers were grown with 9, 11, 13, and 14 ML of Cu. A 20-ML Au cap served to protect the films against oxidation during *ex situ* magnetic characterization. Although thicker Cu films are of less desirable quality, they were necessary in order to observe antiparallel alignment of the magnetizations. Weak RHEED oscillations were observed during the growth of Fe on Cu and Au on Fe.

III. MAGNETIC CHARACTERIZATION AND TRANSPORT MEASUREMENTS

Ferromagnetic resonance (FMR) was used to measure the magnetocrystalline anisotropies in the sample. Measurements were performed in the parallel configuration using a 36-GHz TE_{01} resonant mode. In order to determine the surface anisotropies of single Fe films, a series of samples were prepared consisting of 20Cr/10Cu/XFe/GaAs(100), where X is the number of Fe layers. Analysis was performed using the ultrathin film limit.[21] The validity of this assumption was verified by numerical calculations where the effect of an inhomogeneous rf magnetization and effective field was considered and was found to be negligible for the range of Fe thickness measured in this paper. Each sample was fit according to the Landau-Lifshitz equation[21] with terms including an in-plane fourfold anisotropy K_1, an in-plane uniaxial anisotropy K_u, and an effective demagnetizing field $4\pi M_{\rm eff}$. If the perpendicular uniaxial anisotropy originates only from the surface and contains no bulk contribution then the effective demagnetizing field may be written as

$$4\pi M_{\rm eff} = 4\pi D M_s - \frac{2K_s}{dM_s}, \tag{1}$$

where K_s is the perpendicular surface anisotropy, d is the film thickness, and M_s is the saturation magnetization. D is the demagnetizing factor which is nearly equal to 1 for the range of Fe thickness considered.

The thickness dependence of the fourfold anisotropy could be fit by a constant term representing a bulk contribution and a surface term proportional to 1/thickness. From the slope of Fig. 5(a), the bulk term $K_1^{\rm bulk} = (4.6 \pm 0.3)$ 10^5 erg/cm^3 was found to be within error of the bulk term for Fe, 4.74×10^5 erg/cm^3. The surface contribution $K_1^{\rm surface} = (-5.1 \pm 0.5) 10^{-2}$ erg/cm^2 indicated that the anisotropy would reverse sign below (8 ± 1) ML and create an easy axis along the Fe[110] direction as has been observed by Brockmann *et al.*[23]

Similarly in Fig. 5(b), a bulk term and a surface term could fit the effective demagnetizing field $4\pi M_{\rm eff}$. The bulk term gives a $4\pi M_s$ of (21.55 ± 0.47) kOe in agreement with the bulk magnetization of Fe. The perpendicular surface anisotropy $K_s = (1.72 \pm 0.10)$ erg/cm^2 had its easy axis perpendicular to the surface. By subtracting from the measured anisotropy, the surface anisotropy obtained for Fe/Cu interfaces,[21] 0.62 erg/cm^2, a value for the Fe/GaAs(100) interface was found to be $K_s^{\rm Fe/GaAs} = 1.1$ erg/cm^2. It is interest-

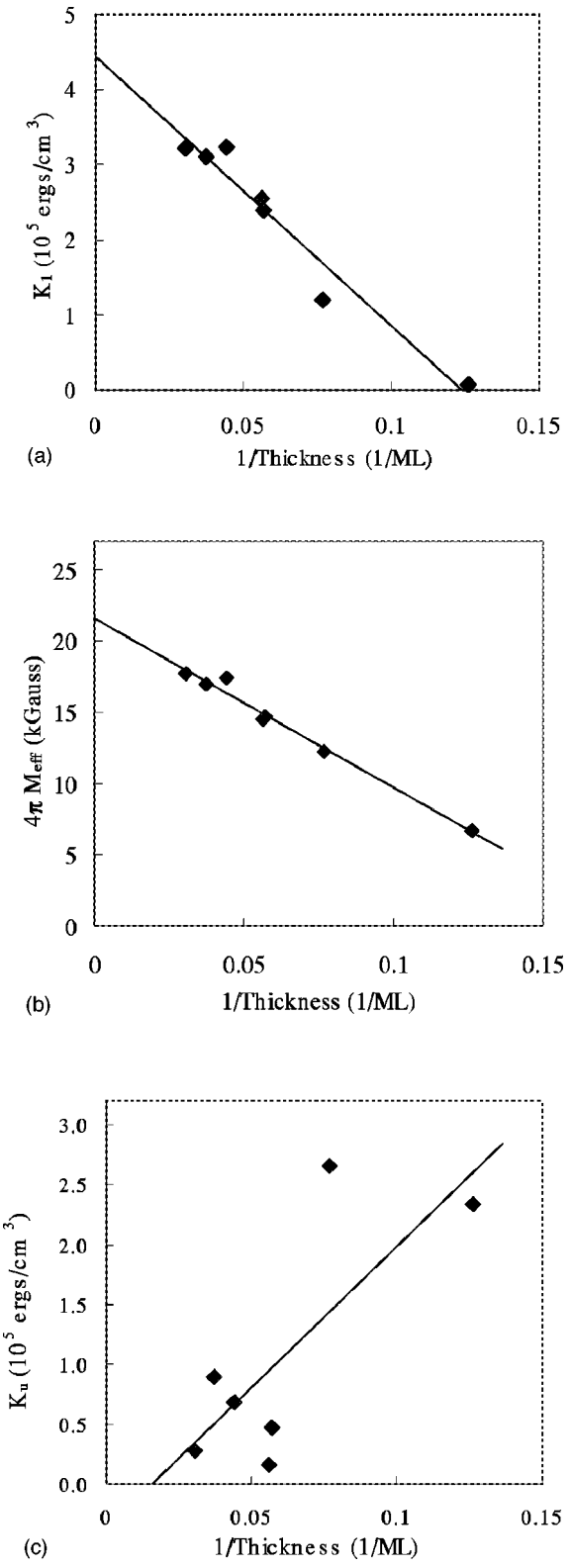

FIG. 5. Thickness dependence of the magnetocrystalline anisotropies for 20Cr/10Cu/XFe/GaAs(100), where X is the thickness of the Fe layer expressed in monolayer (ML). The thickness is given in multilayer format, where the value in front of each element is the number of atomic layers. The solid lines are fits to (a) the fourfold in-plane anisotropy, (b) the effective demagnetizing factor, and (c) the uniaxial in-plane anisotropy.

ing to note that this is even larger than the value for the Fe/vacuum interface, $K_s^{\mathrm{Fe/vacuum}}=0.96\ \mathrm{erg/cm^2}$, which is the largest value so far reported for $3d$ transition-metal interfaces.[22]

As has been found by a number of other groups an in-plane uniaxial anisotropy is present for Fe/GaAs(100). Its orientation is, however, 90° rotated with respect to the direction reported previously for Fe/(4×6)-GaAs(100), with a hard axis along [1-10]. Given the fact that As segregates to the Fe surface regardless of the GaAs(100) reconstruction it is evident that there is significant disruption of the initial GaAs surface. Further studies of the Fe/GaAs interface are required to better interpret the origin of the in-plane uniaxial anisotropy. The uniaxial in-plane anisotropy was found to be sensitive to the precise sample preparation conditions producing large scatter in the data, as has been observed previously.[9,10] The data could be best fit by a term proportional to 1/thickness, which supports the view that the uniaxial anisotropy is created at the Fe/GaAs interface. A value $K_u^{\mathrm{surface}}=(3.2\pm1.2)10^{-2}\ \mathrm{erg/cm^2}$ was obtained from the fit in Fig. 5(c), which is smaller than the value $(12\pm2)10^{-2}\ \mathrm{erg/cm^2}$ measured by Brockmann *et al.*[23] for multiple Fe thickness on a single wafer. Recent STM studies have shown that the (4×6)-GaAs(100) surface as prepared in this paper is a pseudo (4×6) reconstruction comprised of (1×6) domains and (4×2) domains.[14] The amount of each domain is sensitive to the temperature and provides an explanation of the large variations in the uniaxial anisotropy. These results will be presented in a subsequent publication.

FMR measurements were also performed on 20Au/10Fe/13.2Cu/28Fe/GaAs(100) in order to determine the interlayer exchange coupling as well as the anisotropies. Normally a 20Au/10Fe/Cu/GaAs(100) sample would have been prepared in order to determine directly the interlayer exchange coupling in trilayers. This, however, was not possible due to difficulties associated with Cu growth on GaAs(100). The coupling across the 13.2-ML Cu spacer was weak (see below). It turns out that in this limit the in-plane anisotropies are unaffected by the exchange coupling. The size of the fourfold anisotropy of the 28-ML film, $K_1=3.1\times10^5$ erg/cm^3, was as expected from the single Fe layer studies of Fig. 5. The uniaxial anisotropy $K_u=5.0\times10^3\ \mathrm{erg/cm^2}$, however, did not follow the expected trend. The 28 ML was found to be much smaller than expected and was found to have its easy axis +3° away from the [100] direction; this is nearly 45° flipped from what is expected from the single film studies.

The 10-ML film grown on Cu(100) had a fourfold anisotropy $K_1=1.7\times10^5\ \mathrm{erg/cm^3}$, which is 66% of the value obtained for Fe films on Ag(100) substrates.[21] The uniaxial in-plane anisotropy, $K_u=1.0\times10^4\ \mathrm{erg/cm^3}$, had an easy axis roughly +20° away from [100]. The presence of a uniaxial in-plane anisotropy in the Au/Fe/Cu(100) indicates some degree of atomic step ordering in the top Fe film.[24] As can be seen from the FMR measurement shown in Fig. 6, the easy axes are inequivalent, giving rise to a hard-easy and easy-easy axis differing in field by 10 Oe.

Without knowing the perpendicular anisotropy field contribution to the $4\pi M_{\mathrm{eff}}$ for the 10-ML sample, the resonant fields alone were not sufficient to measure the exchange coupling. However, the relative intensities of the resonance

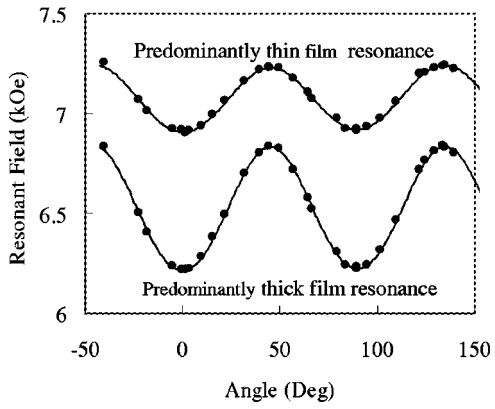

FIG. 6. The resonant FMR fields for 20Au/10Fe/13.2Cu/28Fe/GaAs(100). The films are weakly coupled, therefore one may attribute the high-field resonance predominantly to the thin film and the low-field resonance to the thick film. The angles are plotted with respect to the [100] direction. The curves are fits to the data using the Landau-Lifshitz equation. Note that the sample has an easy-easy axis at 0° and a hard-easy axis at 90°.

peaks could be used to fit the exchange coupling and the perpendicular anisotropy field of the 10-ML Fe film by comparison to calculations.[21] The fit in Fig. 7(a) indicated that the coupling was ferromagnetic with a coupling strength of $+0.005$ erg/cm^2 and the effective demagnetizing field for the 10-ML Fe was $4\pi M_{\text{eff}}=14.55$ kG which is within 10% of the value expected for Au/Fe/Cu(100) interfaces.[21]

Magnetoresistance and longitudinal MOKE measurements of 20Au/10Fe/Cu/28Fe/GaAs(100) were performed along the easy axes in order to study the low-field behavior of the magnetization. These studies were performed on patterned films in order to simultaneously measure Kerr effect and magnetoresistance. The patterning was achieved by Ar^+ etching through a Mo mask, allowing four-probe measurements over a region 0.5×1.2 mm. The inequivalence between the easy axes observed in FMR was also present in the MOKE data. The MOKE measurements from 9- and 11-ML samples showed very simple single jump hysteresis loops, indicating that the exchange coupling was ferromagnetic.

The hysteresis from the 13.2-ML sample had a much more interesting magnetization curve. Interpretation of the MOKE data was obscured by the presence of relatively large hysteresis, as seen in the magnetization loops of Fig. 8(a). In order that the field dependence of magnetization follow the minimum energy, a gradually increasing and decreasing ac in-plane magnetic field was applied perpendicular to the dc field between successive increments of the dc field. The ac field had an amplitude of roughly 100 Oe at a driving frequency of 300 Hz. The fact that the hysteresis is removed in Fig. 8(b) proves that the magnetization follows the minimum energy for each given value of applied dc field. The magnetization curve from a sample with a 13.2-ML Cu spacer shows two well defined jumps between zero applied field and saturation. These are labeled H_1 and H_2 in Fig. 8(b). Most surprising is the fact that the shape of the magnetization curves are characteristic of antiferromagnetic coupling, even though coupling measured by FMR was ferromagnetic.

When the sample was magnetized along the hard-easy axis, the MOKE signal in zero applied field dropped to a plateau corresponding to the magnetization jumping 90° to

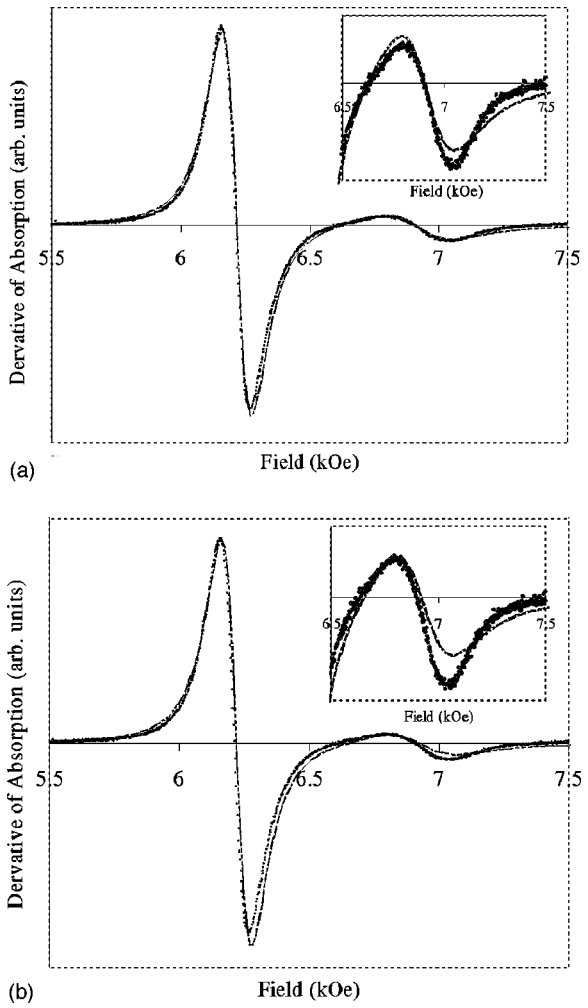

FIG. 7. FMR along the easy axis for 20Au/10Fe/13.2Cu/28Fe/GaAs(100). A value of $J_{\text{eff}}(0)=+0.005$ erg/cm^2 was obtained from the fit of the two peaks in (a), and is compared to the curve (b), the signal expected for the coupling $J_{\text{eff}}(0)=-0.012$ erg/cm^2 obtained by fitting the magnetoresistance using only bilinear and biquadratic coupling. Dots are experiment; solid lines are calculations.

the easy-easy axis in an antiparallel configuration. This is the lowest energy for the system. As expected, such a plateau was not observed during magnetization reversal along the easy-easy axis. The observation of a weak inequivalence in easy axes using the Kerr effect is a demonstration that the anisotropy measurements which were taken at high fields in FMR are applicable to the low-field MOKE measurements.

Trilayers with a 13.2-ML Cu spacer exhibited respectable GMR ratios. This was also surprising, given the FMR data, since the existence of GMR requires the angle between the magnetizations to vary with field, something which does not normally occur for ferromagnetic coupling. The size of the magnetoresistance $R\%=[R(H=0)-R(H_{\text{sat}})]/R(H_{\text{sat}})$ was found to be 2.0% at room temperature and 5.5% at 4 K. The magnetoresistance had a one-to-one correspondence with the Kerr effect data. For room-temperature measurements with the current parallel to both the applied field and the hard-easy axis, the GMR showed a 0.11% drop in resistance shown in Fig. 8(c). This corresponded to the zero-field plateau observed in MOKE. In zero applied field the magnetization lies along the easy-easy axis, perpendicular to the cur-

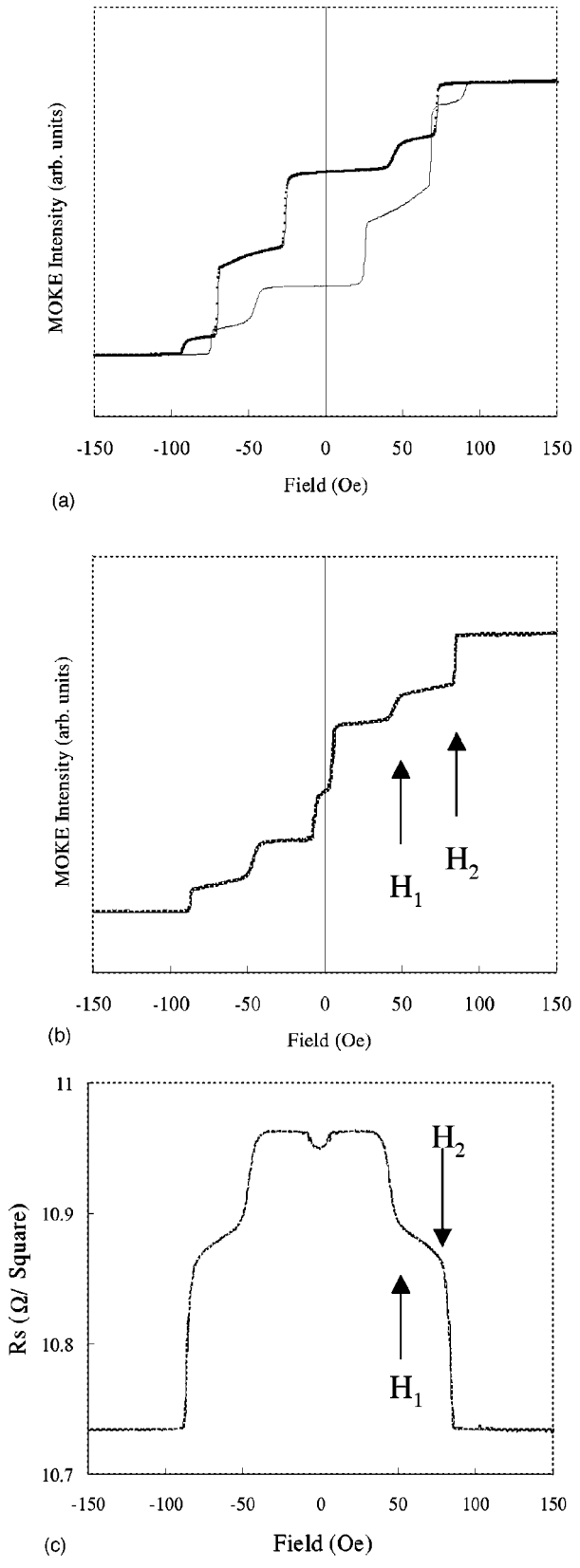

FIG. 8. (a) The MOKE hysteresis loops for 20Au/10Fe/13.2Cu/28Fe/GaAs(100). (b) shows the MOKE magnetization curve for the same sample with the hysteresis removed by a transverse ac field. The applied dc magnetic field is in both the plane of the sample and the plane of incidence. The sheet resistance as a function of field was recorded simultaneously and is presented in (c) for the current parallel to the applied field.

rent, giving rise to a decrease in resistance through anisotropic magnetoresistance. This was verified by measuring the difference between the resistance with the saturation field parallel to the current $R_{\parallel}$, and perpendicular to the current $R_{\perp}$. At room temperature, $R_{\parallel}=25.91\,\Omega$ and $R_{\perp}=25.83\,\Omega$, which results in an anisotropic magnetoresistance (AMR) ratio of $(R_{\parallel}-R_{\perp})/R_{\text{average}}=0.3\%$ in agreement with the value previously reported for Fe/GaAs(100).[25] The fact that the AMR at saturation was larger than the zero-field drop in resistance indicated that in the ground state the magnetization was distributed between the two easy axes. This indicated that there was some inhomogeneity in the uniaxial anisotropy, however, the uniaxial anisotropy amounts to only a few percent of the total anisotropy and should therefore play a small role in the behavior of the magnetization for nonzero applied fields.

As compared to Co/Cu and Cr/Fe systems, the 5.5% GMR is relatively small. However, the GMR is not expected to be large, due to a mismatch between the electronic band structures of Cu and Fe.[26] Sputtered (15-Å Fe/15-Å Cu)$_{60}$ multilayers grown on Si(100) have a 2.6% GMR at room temperature,[27] which is comparable to our results. Our GMR in Fe/Cu/Fe/GaAs(100) is relatively large if one considers that multilayers may have an enhanced magnetoresistance due to a reduction of diffuse scattering at the outer surfaces. Theoretically, for a 10-Å nonmagnetic spacer, a multilayer GMR can expect a fivefold enhancement over trilayers.[28] Furthermore, the Fe/Cu multilayers do have a stronger temperature dependence: the magnetoresistance increases fivefold as the temperature is dropped to 4 K, compared to a 2.8-fold increase in Fe/Cu/Fe/GaAs(100).

IV. DISCUSSION

Quantitative analysis of the exchange coupling present in the MOKE and GMR data was made by comparison to minimum-energy calculations using the theory in Ref. 29. The values for the magnetocrystalline anisotropies used in the calculation were those obtained by FMR measurements. The interlayer exchange energy as a function of the angle θ between the magnetization of the two films, was initially assumed to be of the form

$$E_{\text{exch}}=-J_1\cos\theta+J_2\cos^2\theta. \tag{2}$$

The total effective coupling in the magnetic torque is thus

$$J_{\text{eff}}(\theta)=J_1-2J_2\cos\theta. \tag{3}$$

The bilinear coupling J_1 and biquadratic coupling J_2 were used as fitting parameters. MOKE data are known to be difficult to interpret quantitatively, especially for noncollinear configurations of the magnetic moments.[30] Since the magnetoresistance is expected to have a simple $\cos^2(\theta/2)$ angular dependence, the GMR data were compared to the calculations. $J_1=-0.0166$ and $J_2=0.0022\,\text{erg/cm}^2$ were able to fit the critical fields H_1 and H_2 as shown by the dashed line in Fig. 9(a).

Calculations predict that the thick film will deviate no more than 3° from the applied field direction when the total magnetic moment of the 10-ML film $\mathcal{M}_{\text{thin}}$ and the moment of the 28-ML film $\mathcal{M}_{\text{thick}}$, are noncollinear. Once the field is

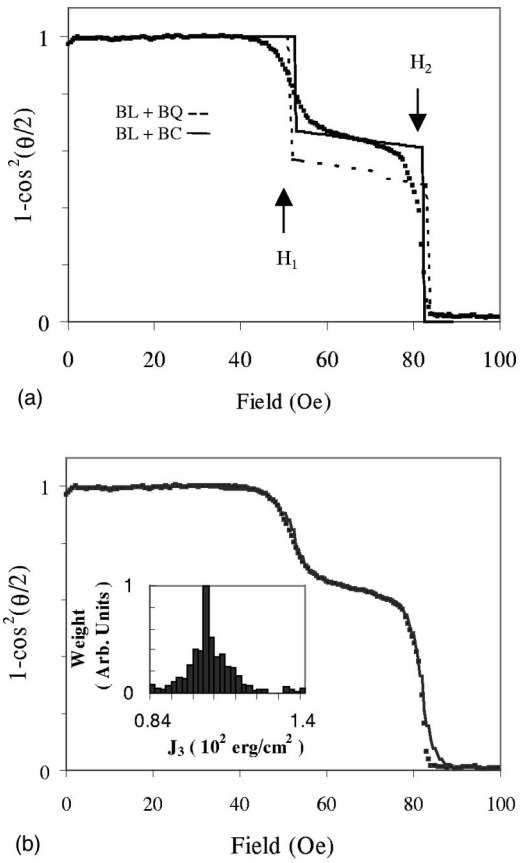

FIG. 9. Fits of the GMR data are used to measure the interlayer exchange coupling. (a) The solid line is the fit using bilinear and bicubic exchange coupling ($BL+BC$) $J_1=-0.0277$, $J_2=0$, and $J_3=0.01$ erg/cm^2. The dashed line is the fit using purely bilinear and biquadratic coupling ($BL+BQ$), $J_1=-0.0166$ and $J_2=0.0022$ erg/cm^2. (b) A weighted average of calculated GMR curves with coupling strengths $J_1=-0.0277$ erg/cm^2 and J_3 ranging from 0.0084–0.0140 erg/cm^2. The inset represents the relative weights given to each coupling strength.

lowered to the field H_2, $\mathcal{M}_{\text{thin}}$ jumps over a hard axis, and is temporally caught by the anisotropy in a noncollinear configuration. When the field has fallen below a critical value H_1, the magnetization of the 10-ML film jumps over the second hard axis into an antiparallel configuration. The angle between the magnetizations in the noncollinear regime was, however, higher than that expected from the calculation.

It is worth noting the importance of the magnetocrystalline anisotropies in the magnetization reversal. The cubic anisotropy is comparable to the total effective exchange coupling found here. An estimate of the effective exchange field may be obtained by taking the limit of small-angle rotation from a parallel configuration,

$$H_{\text{ex}}=\frac{J_1-2J_2}{M_s}\left(\frac{1}{d_A}+\frac{1}{d_B}\right), \tag{4}$$

where d_A and d_B are the thickness of the magnetic layers and M_s is the saturation magnetization. From the values of coupling obtained from GMR, $H_{\text{ex}}=120$ Oe. This is smaller than both the effective fields from the cubic anisotropies: $2K_l/M_s=200$ and 370 Oe for the 10- and 28-ML films, respectively. As a result the anisotropy will play an important role in the behavior of the magnetization reversal and insures that the magnetic moments do not deviate far from the easy axes. It is the magnetocrystalline anisotropies which are responsible for the discontinuous jumps at H_1 and H_2.

There were two sources of discrepancy between the data and a model assuming bilinear and biquadratic exchange. The first was a disagreement between measured and calculated angles between $\mathcal{M}_{\text{thin}}$ and $\mathcal{M}_{\text{thick}}$. Calculations showed that the net effect of J_1, J_2 and the anisotropies caused $\mathcal{M}_{\text{thin}}$ to jump 86° with respect to the applied field at the critical field H_2. $\mathcal{M}_{\text{thick}}$ made a small rotation such that the angle between the magnetizations was 88°. This was in contrast to the GMR data in Fig. 9 which indicated that at H_2, $\mathcal{M}_{\text{thin}}$ jumped to make an angle $\theta=98°$ with respect to $\mathcal{M}_{\text{thick}}$.

The second cause for concern was the fact that the total coupling at saturation $J_{\text{eff}}(0)=J_1-2J_2=-0.012$ erg/cm^2 was antiferromagnetic, opposite to the FMR measurements. The expected FMR signal from $J_{\text{eff}}(0)=-0.012$ erg/cm^2 is shown to be in disagreement with experiment in Fig. 7(b). These two points of disaccord casted doubt on a purely bilinear and biquadratic description of the interlayer exchange.

Higher-order coupling J_3 was introduced in Eq. (2) in attempt to reconcile the disagreements:

$$E_{\text{exch}}=-J_1\cos\theta+J_2\cos^2\theta-J_3\cos^3\theta. \tag{5}$$

The total effective coupling thus becomes

$$J_{\text{eff}}(\theta)=J_1-2J_2\cos\theta+3J_3\cos^2\theta. \tag{6}$$

A fit of the GMR data is shown in Fig. 9(a) with exchange coupling constants $J_1=-0.0277$, $J_2=0.0$, and $J_3=0.0104$ erg/cm^2. The first point to note is that both the positions of the critical fields H_1 and H_2 and the angle between the magnetizations were able to be explained by the addition of J_3 coupling. Second, at saturation the total effective coupling $J_{\text{eff}}(0)=J_1-2J_2+3J_3=+0.0035$ erg/cm^2 is positive, in accord with the FMR data. The total effective coupling $J_{\text{eff}}(\theta)$ does become negative for $15°<\theta<160°$, however, it is interesting to note that the total effective coupling for antiparallel orientations of the magnetic moments is again positive, $J_{\text{eff}}(180°)=J_1+2J_2+3J_3=+0.0035$ erg/cm^2. This is a surprising result considering that the ground state is in an antiparallel configuration. Such a situation has not been observed yet in any system, and requires further deliberations. To fully understand the magnetization reversal, minimum-energy calculations must be performed. By minimizing only the exchange energy with respect to the angle θ, using the coupling constants shown above, one sees that the net effect of J_1 and J_3 would be to hold $\mathcal{M}_{\text{thin}}$ at an angle 160° with respect to $\mathcal{M}_{\text{thick}}$. In order to determine the angular dependence of the magnetic moments as a function applied field, the anisotropies must also be considered. As the field is lowered to the critical field H_2, $\mathcal{M}_{\text{thin}}$ jumps in the direction of the minimum of the exchange energy. H_2 is only weakly dependent on the in-plane anisotropy of the thin film. Calculations show that even without anisotropy a jump occurs at H_2 with an angle of $\theta=115°$. The presence of a fourfold anisotropy reduces this angle to 98°. With further decreasing field, $\mathcal{M}_{\text{thin}}$ rotates in the direction of the exchange energy minimum. However, the presence of the mag-

netocrystalline hard axis at 145° provides a barrier over which $\mathcal{M}_{\text{thin}}$ must jump in order to reach 160°. It turns out that the magnetocrystalline anisotropy is strong enough such that $\mathcal{M}_{\text{thin}}$ jumps not to 160°, but rather to an antiparallel configuration with the magnetic moments collinear with the applied magnetic field and the easy crystalline axis. This happens despite the fact that for small-angle rotations, the exchange coupling in this configuration is ferromagnetic. The effective exchange field felt for small angle rotation from an antiparallel configuration is given by

$$H_{\text{ex}}=\frac{J_1+2J_2+3J_3}{M_s}\left(\frac{1}{d_A}+\frac{1}{d_B}\right). \tag{7}$$

For the coupling measured by GMR, $H_{\text{ex}}=20\,\text{Oe}$, which is far less than the effective fields due to the cubic anisotropies of either Fe film. Therefore at zero field the magnetocrystalline anisotropy will dominate and create an antiparallel alignment of the magnetic moments.

The discrepancy between the coupling strengths measured by GMR and FMR may be explained by considering inhomogeneity in the sample. The fact that the jumps in magnetoresistance shown in Fig. 9 are not perfectly sharp is indicative of inhomogeneity. By varying the anisotropies and coupling constants input into the calculation of the GMR curves, the width of the jumps in magnetoresistance was seen to be due to inhomogeneous J_3 coupling. A weighted average of calculated GMR curves with coupling strengths ranging from $J_3=0.0084-0.0140\,\text{erg/cm}^2$ is present in Fig. 9(b). Note that the broadening of the jump in resistance at the critical field H_1 is larger than that at H_2 and is accurately described by the calculation. This could not be modeled by an inhomogeneous bilinear coupling for which calculations show broadens both the critical fields H_1 and H_2. Variations in the fourfold anisotropy were also unable to describe the broadening of the switching fields. Since the fourfold anisotropy of the thin film A affected little the critical field H_2 an inhomogeneous distribution of its value would produce a sharp jump at a field H_2 and therefore would not account for the broadening present in the data. The uniaxial anisotropy was small, and variations in its value resulted in only small changes in the switching fields. The bicubic coupling was the only single parameter whose variations could accurately model the data. The distribution in the bicubic coupling furthermore brings FMR and GMR into more quantitative agreement. The distribution in bicubic coupling shows that the total effective exchange coupling measured by FMR is within the range of values of $J_{\text{eff}}(0)=(0.0035\pm0.0012)$ erg/cm^2 determined from GMR. Differences in values measured by these two techniques is due to the fact that FMR measures over an area 2×3 mm determined by the sample size of the film, whereas GMR measures over an area determined by the patterning, 0.5×1.2 mm.

Interestingly, the coupling in our samples is ferromagnetic for small-angle rotations. The change in the sign of the coupling implied that as the external field was lowered from saturation, large-angle fluctuations of the magnetization were needed to bring the thin film away from parallel alignment with the thick film, into a lower energy state. This was accomplished through the application of the transverse field described previously.

It is interesting to compare the results with trilayers grown on other substrates. The exchange coupling of Fe/Cu/Fe was also measured for samples grown on Ag(100).[31] In these samples only long-wavelength coupling was observed. The existence of short-wavelength oscillations in exchange coupling through a Cu(100) spacer was present in the biquadratic exchange coupling, which was increasing with increasing size of atomic terraces in agreement with Slonczewski's model.[32] The smoothness of Cu samples prepared on Ag substrates were noticeably better than for Cu grown on Fe/GaAs(100) as indicated by RHEED patterns and RHEED intensity oscillations. This was evident in the measured values of the bilinear and biquadratic exchange coupling. In the same thickness range as the trilayers grown on GaAs, the bilinear coupling was roughly an order of magnitude larger in the case of Fe/Cu/Fe/Ag(100). This difference is explained by interface roughness since J_1 is an algebraical average of positive and negative bilinear exchange coupling from local variations in the spacer thickness. J_2, which creates a tendency to orient the magnetic moments perpendicularly, originates from magnetic frustrations due to lateral variations in positive and negative coupling between Fe layers. The absence of biquadratic coupling in Fe/Cu/Fe/GaAs(100) is consistent with Slonczewski's model since J_2 decreases quadratically with the Fe/Cu interface roughness [see Equation (2.17) in Ref. 21].

The origin of the bicubic interlayer exchange coupling is in question. The positive value of J_3 creates a tendency for parallel coupling. Given the negative sign of J_1, it is reasonable to expect that there is also a residual ferromagnetic bias in the next higher-order term in an angular dependent expansion of the exchange coupling. The presence of J_3 in Fe/Cu/Fe/Ag(100) samples was difficult to detect since the size of J_1 and J_2 were considerably larger than was the case for trilayers grown in GaAs(100). In fact the significantly reduced values of J_1 and J_2 observed for trilayers grown on GaAs enabled the observation of the bicubic term J_3.

V. CONCLUSION

A procedure has been presented to prepare Fe surfaces on GaAs(100), yielding a template for growing high quality structures for magnetoresistance studies. By removing As from the Fe surface, lower step density surfaces could be achieved. XPS suggests that there may be 0.2–0.3 ML of Ga diffusion into the Fe as a result of cascade mixing from sputtering. The magnetic anisotropies of the Fe thin films have been found to be composed of a surface and a bulk contribution. The bulk terms were equal to the values of bulk Fe. Epitaxial Cu in Fe/Cu/Fe trilayers could only be prepared by cooling during the copper growth. Broad RHEED features show that the Cu layer is rougher than was observed for the room-temperature growth of Cu layers on Fe/Ag(100). The trilayers were measured by FMR, which is a high-field technique, and by MOKE and GMR which are low-field techniques. The good agreements between the results obtained from each method indicates that the high-field measurements of anisotropies are applicable to the analysis of magnetization and magnetoresistance curves. For exchange coupled

Fe/13.2Cu/Fe/GaAs(100), a 2.0% room-temperature GMR ratio was observed, which is comparable to Fe/Cu multilayers prepared by sputtering. This represents a significant GMR if the factor of enhancement due to multilayer structures is expected to be fivefold. The anisotropic magnetoresistance was found to be 0.3% in these samples.

The coupling as measured by ferromagnetic resonance and giant magnetoresistance could not be explained simply by bilinear and biquadratic exchange alone. A phenomenological coupling parameter that varies as the cube of the cosine of the angle between the magnetic moments, bicubic exchange, has been proposed to explain the field dependence of the GMR. Further studies are required to determine whether the origin of bicubic interlayer exchange is intrinsic or extrinsic. In the case of Fe/Cu/Fe on GaAs, the bicubic exchange coupling is comparable in strength to the bilinear coupling which leads to an unexpected experimental result. GMR and MOKE shows noncollinear coupling in low magnetic fields, and FMR shows ferromagnetic coupling where measurements are performed at fields well above saturation.

[1] S. S. P. Parkin, Phys. Rev. Lett. **71**, 1641 (1993).
[2] S. A. Chambers, F. Xu, H. W. Chen, I. M. Vitomirov, S. B. Anderson, and J. H. Weaver, Phys. Rev. B **34**, 6605 (1996).
[3] G. W. Anderson, M. C. Hanf, X. R. Qin, P. R. Norton, K. Myrtle, and B. Heinrich, Surf. Sci. **346**, 145 (1996).
[4] A. Filipe and A. Schuhl, J. Appl. Phys. **81**, 4359 (1997).
[5] T. L. Monchesky, B. Heinrich, S. Watkins, and P. Yeo (unpublished).
[6] A. Filipe, A. Schuhl, and P. Galter, Appl. Phys. Lett. **70**, 129 (1997).
[7] M. Zölfl, M. Brockmann, M. Köhler, S. Kreuzer, T. Schweinböck, S. Miethaner, F. Bensch, and G. Bayreuther, J. Magn. Magn. Mater. **175**, 16 (1997).
[8] Y. B. Xu, E. T. Kernohan, D. J. Freeland, A. Ecrole, M. Tselepi, and J. A. C. Bland, Phys. Rev. B **58**, 890 (1998).
[9] J. J. Krebs, B. T. Jonker, and G. A. Prinz, J. Appl. Phys. **61**, 2596 (1987).
[10] M. Gester, C. Daboo, R. J. Hicken, S. J. Gray, A. Ercole, and J. A. C. Bland, J. Appl. Phys. **80**, 347 (1996).
[11] G. W. Anderson, M. C. Hanf, P. R. Norton, M. Kowalewski, K. Myrtle, and B. Heinrich, J. Appl. Phys. **79**, 4954 (1996).
[12] E. M. Kneedler, B. T. Jonker, P. M. Thidabo, R. J. Wagner, B. V. Shanabrook, and L. J. Whitman, Phys. Rev. B **56**, 8163 (1997).
[13] W. F. Egelhoff, Jr., P. J. Chen, C. J. Powell, M. D. Stiles, R. D. McMichael, J. H. Judy, K. Takano, and A. E. Berkowitz, J. Appl. Phys. **82**, 6142 (1997).
[14] T. L. Monchesky, R. Urban, B. Heinrich, M. Klana, and J. Kirschner (unpublished).
[15] P. M. Thibado, E. Kneedler, B. T. Jonker, B. R. Bennett, B. V. Shanabrook, and L. J. Whitman, Phys. Rev. B **53**, R10 481 (1996).
[16] S. Tanuma, C. J. Powell, and D. R. Penn, Surf. Interface Anal. **17**, 911 (1991).
[17] P. Sigmund, in *Sputtering by Particle Bombardment I*, edited by R. Behrisch (Springer-Verlag, Berlin, 1981).
[18] Z. Celinski and B. Heinrich, J. Appl. Phys. **70**, 5935 (1991).
[19] J. Unguris, R. J. Celotta, D. A. Tulchinsky, and D. T. Pierce, J. Magn. Magn. Mater. **198-199**, 396 (1999).
[20] J. Bonin, Ph.D. thesis, Simon Fraser University, 1993.
[21] B. Heinrich and J. F. Cochran, Adv. Phys. **42**, 523 (1993).
[22] K. Urquhart, B. Heinrich, J. F. Cochran, A. S. Arrott, and K. Myrtle, J. Appl. Phys. **64**, 5334 (1988).
[23] M. Brockmann, S. Miethaner, M. Zölfl, and G. Bayreuther, J. Magn. Magn. Mater. (to be published).
[24] B. Heinrich, S. T. Purcell, J. R. Dutcher, K. Urquhart, J. F. Cochran, and A. S. Arrott, Phys. Rev. B **38**, 12 879 (1988).
[25] F. J. Rachford, M. Rubinstein, and G. A. Prinz, J. Appl. Phys. **63**, 4291 (1988).
[26] B. Dieny, J. Magn. Magn. Mater. **136**, 335 (1994).
[27] F. Petroff, A. Barthélemy, D. H. Mosca, D. K. Lottis, A. Fert, P. A. Schroeder, W. P. Pratt, Jr., R. Loloee, and S. Lequien, Phys. Rev. B **44**, 5355 (1991).
[28] B. Dieny, J. Phys.: Condens. Matter **4**, 8009 (1992).
[29] J. F. Cochran, J. Magn. Magn. Mater. **147**, 101 (1995).
[30] R. M. Osgood III, B. M. Clemens, and R. L. White, Phys. Rev. B **55**, 8990 (1997).
[31] B. Heinrich, Z. Celinski, J. F. Cochran, A. S. Arrott, K. Myrtle, and S. T. Purcell, Phys. Rev. B **47**, 5077 (1993).
[32] J. Slonczewski, Phys. Rev. Lett. **67**, 3172 (1991).